Journal of Environmental Health Science and Engineering (2023) 21:239–254
https://doi.org/10.1007/s40201-023-00858-x

RESEARCH ARTICLE

Ppy/TiO_2-SiO_2 nanohybrid series: synthesis, characterization, photocatalytic activity, and antimicrobial potentiality

Meena Yadav[1] · Rajat Arora[1] · Monika Dhanda[1] · Simran Ahlawat[1] · Sachin Shoran[2] · Suman Ahlawat[3] · Satya Pal Nehra[2] · Geeta Singh[4] · Suman Lata[1]

Received: 25 July 2022 / Accepted: 8 April 2023 / Published online: 25 April 2023

Abstract

A series of polypyrrole doped TiO_2-SiO_2 nanohybrids (Ppy/TS NHs) were synthesized thru in-situ oxidation polymerization by varying weight ratio of pyrrole. The structural analysis of NHs were characterized by X-ray Diffraction (XRD) spectra, UV-visible (UV-Vis) spectra and X-ray Photoelectron spectra (XPS) confirmed synthesis of nanomaterials. Surface and morphological study done by adopting, Scanning Electron Microscopy (SEM), Energy Dispersive Spectroscopy (EDS), Transmittance Electron Microscopy (TEM) and Brunauer-Emmett-Teller (BET) analysis confirmed the homogenous distribution, nano range size formation and mesoporous nature of nanohybrids. Further, electrochemical behavior of synthesized NHs investigated by adopting Electrochemical Impedance Spectroscopy (EIS) showed good kinetic behaviour and electron transport tendency. The nanohybrids and precursors were examined for photocatalytic degradation of methylene blue (MB) dye and revealed enhanced degradation tendency for the NHs series photocatalysts. It was found that variation of pyrrole (0.1 to 0.3 g) to TS nanocomposites (TS Nc) increased the photocatalytic potential of TS Nc. The maximum photodegradation efficacy was found to be 90.48% in 120 min for Ppy/TS0.2 NHs under direct solar light. Additionally, Ppy/TS0.2 NHs performed appreciably towards antibacterial studies against some Gram-positive and Gram-negative deleterious bacteria, Escherichia coli, Klebsiella pneumoniae, Staphylococcus aureus, Shigella flexneri microbes.

Keywords Ppy/TS nanohybrids · Methylene Blue dye · Photocatalytic degradation · Antibacterial probing

Introduction

Recently, metal oxide nanomaterial and their polymeric nanocomposites advanced environmental and electrochemical studies are becoming ubiquitous depending upon their diverse photo-chemical, bio-compatible and electro-catalytic behavior reliant to their stability, nano size, and improved surface area [1, 2]. Such materials have been reported for various applications such as waster disinfection [3], solar cell [4], energy storage [5], biosensing [6], corrosion [7], antimicrobial study [8] and many more. Water disinfection is the major issue and an essential necessity for sustainable life. Currently, humankind is on its best time in the terms of socialization and vogue. To maintain the vogue, industries are doing their best. But then the secretion of various pollutants like heavy metals, poisonous gases and organic dyes contaminate the aquatic system. Moreover, organic waste released from paper, leather, textile, pharma, and beverage industries always have high concentration of harmful pollutants [9]. Then again there is a vast problem of dye discard around us. The dyes are very detrimental for the entire living species. Once, they get dissolved into water, it is rather impossible to remove the dye from the water. Various industries discard dye water intrinsically into rivers and other water bodies and that leads to threatening to marine bodies and humankind. Dye solutions block the oxygen exchange in water bodies by forming a layer onto the top of water surface. The problem does not end here, the indigestion of dye

✉ Suman Lata
sumanjakhar.chem@dcrustm.org

1 Department of Chemistry, Deenbandhu Chhotu Ram University of Science and Technology, Murthal 131039, Haryana, India

2 Center of Excellence for Energy and Environmental Studies, Deenbandhu Chhotu Ram University of Science and Technology, Murthal, Haryana 131039, India

3 Department of Chemistry, Maharshi Dayanand University, Rohtak 124001, India

4 Department of Biomedical Engineering, Deenbandhu Chhotu Ram University of Science and Technology, Murthal 131039, Haryana, India

water by marine bodies leads to noxiousness in them which further leads to biomagnification in the other species [10].

Subsequently, the need of the day is to remove the dye contamination from water. The most easy and contingent way to degrade the dyes is photocatalytic degradation. Photocatalytic degradation is the degradation of a substance in the presence of solar light or UV-vis light. The extent of photocatalytic activity varies with the capacity of the photocatalyst to generate electron-hole pairs, which harvest free radicals by contributing to secondary reactions. A semiconductor material can perform as a photocatalyst by absorbing a photon of energy analogous to its band gap, creating electron-hole pairs, which are then divided and shifted to the target pollutant for redox reaction [11]. Currently, various physical, chemical, and biological studies have been approached to remove non-biodegradable organic pollutants and microbial contamination from water [9]. Now-a-days, conducting polymers and metal oxides based nanomaterials as photocatalyst are of great research interest among researchers [12]. Various metal oxides-based nanocomposites are deliberately used in photodegradation application [13–16]. TiO_2 nanoparticles are preferred among such a large choice due to its nontoxic nature, larger surface area and oxygen storage, biocompatible and electrocatalytic nature [17, 18]. In order to enhance photodegradation tendency, TiO_2 nanoparticles are combined with few mesoporous matters like SiO_2, Al_2O_3 owning to their electrocatalytic and photocatalytic properties [19, 20]. These materials are low cost, easily synthesized and can be exploited for environmental, energy and electrochemical applications [21, 22]. Further, these nanocomposites are intercalated with polymeric material to form nanohybrids.

From literature, various conducting polymers-based composites are being used for solar cells, supercapacitors, sensors and biosensors, water treatment, corrosion inhibition and many more applications [4, 5, 23, 24]. Among several polymers, the authors have selected polypyrrole (Ppy) due to its high conductivity, simplistic synthesis, photocatalytic and ecofriendly nature [25–27]. Kumar et al. reported ternary TiO_2/PANI/GO nanocomposites based comparative study for photocatalytic degradation of Rose Bengal Dye under visible light [24]. Ppy, being a conducting polymer, provides easier intercalation of binary hybrid of metal oxides into the matrix, thereby enhancing its electrical, optical, photochemical, and catalytic properties. While SiO_2 being a mesoporous material offers better adsorption tendency and catalytic properties. Such heterostructures offer precise control over charge carriers' movement. In present work, a series of Ppy/TiO_2-SiO_2 nanohybrids have been synthesized through doping different concentrations of Ppy and employed for photocatalytic degradation of Methylene Blue dye in direct solar light, supplemented with one more application of the nanohybrids as their antimicrobial behavior. The novelty of the study lies in the fact that these hybrids, being environment friendly, are synthesized for the first time and have not been investigated so far for both the applications.

Materials and methods

Test materials and chemicals

Titanium tetraisopropoxide (TTIP), Tetraethylorthosilicate (TEOS) both (99.99%) from CDH, Pyrrole (99.98%), Dimethylformamide (99.7%), Ferric chloride (99.9%), Sulphuric acid (98% assay), Ethanol, Potassium hydroxide (KOH), Potassium chloride (KCl) (rest all 99.9%) and methylene blue dye were obtained from Thermo Fischer Scientific India Pvt. Ltd. All chemicals procured were of analytical research grade. Pyrrole was distilled to remove impurities although rest of the chemicals were consumed without any further purification. All synthesis and analysis were completed using ultrapure doubly distilled water.

Synthesis of TiO_2-SiO_2 nanocomposites

TiO_2-SiO_2 nanocomposites (TS Nc) were synthesized by using previously reported modest and simplistic sol-gel method [21]. Titanium tetraisopropoxide (TTIP) and tetraethylorthosilicate (TEOS) were used as precursors. Initially, TTIP, ethanol and ultrapure distilled water were taken in stoppered conical flask (250 mL) in 2.2:1.0:2.9 mol ratio, respectively and stirred until homogenization. Amid, 1 mL KOH solution of 1 N concentration was dropped in to make solution alkaline. During sol-gel process, few particles were detected [17]. Afterward, TEOS, ethanol and ultrapure distilled water were taken in 1.5:7.5:6.0 mol ratio, respectively and transferred in above mixture again followed by stirring for~ 30 min [28]. During stirring, once again 1 mL KOH solution of 1 N concentration was poured and a translucent sol was formed. Lastly, the solution left overnight to settle down as gel at room temperature. At the end, the gel thus formed was calcined at 500 ℃ for 2 h to eliminate any unstable impurity. Later, TS Nc were stored in a moisture free environment for further amendment.

Synthesis of Ppy/TiO_2-SiO_2 nanohybrids

Ppy/TS NHs were synthesized by in-situ oxidation polymerization method [7]. Initially, a certain amount of binary TS Nc was ultrasonicated in 20 mL methanol for 30 min. Then, 40 mL of methanol and distilled water each were taken in beaker and stirred for 5 min on magnetic stirrer and mixed with above ultrasonicated mixture. While stirring x = 0.1 g, 0.2 and 0.3 g of pyrrole was added drop wise to above solution and again stirred for 10 min. Meanwhile, 40 mL of 1.0 M $FeCl_3$ solution was poured gradually into above mixture and stirred for 6 h. Throughout the whole experiment, a temperature beneath 0 ˚C was maintained [25, 29]. Afterwards, the black precipitates obtained were washed with methanol

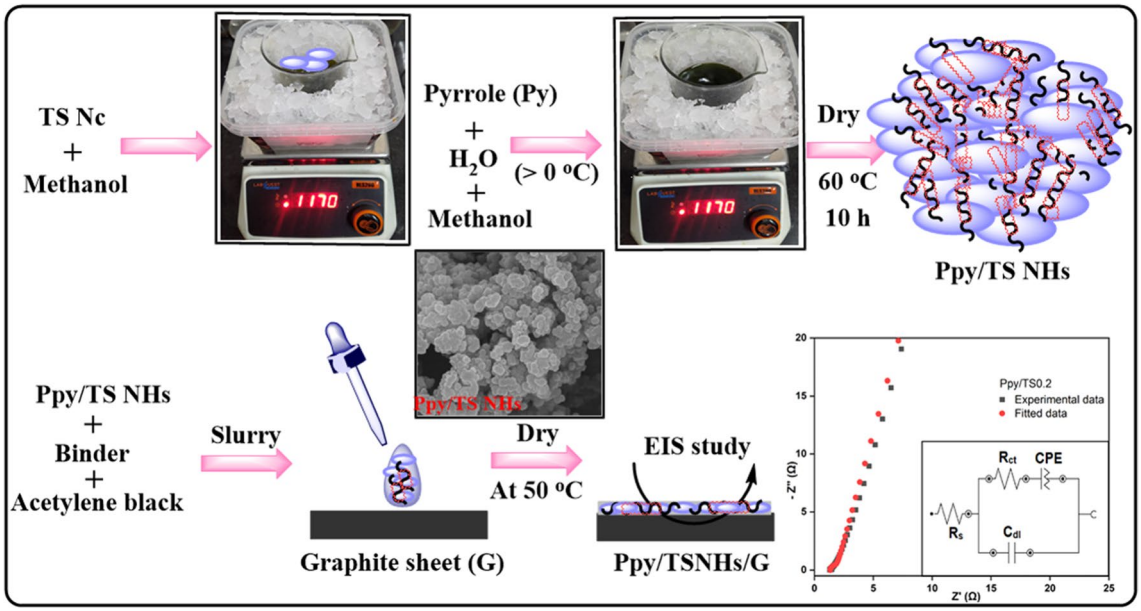

Scheme 1 Schematic illustration of PPy/TiO_2-SiO_2 nanohybrids synthesis

and dried for 10 h at 60 °C schematically represented in Scheme 1.

Characterization techniques

Structural characterizations

X-ray Diffraction analysis with Rigaku Ultima D8 advance was done to achieve phase parameter and structural study. UV-Visible spectrophotometer, Analytical UV 3092 by LABINDIA (DCRUST, India) ranging 200 to 800 nm was adopted for optical activity and photocatalytic degradation study of photocatalysts. XPS was achieved to determine oxidation state and elemental composition of nanocomposites and Ppy/TS0.2 nanohybrids by using PHI 5000 Versa Probe III (CRF IITD, Sonepat campus).

Surface and morphological characterizations

Surface morphology of synthesized TS Nc and best Ppy/TS0.2 NHs samples was examined by Field Emission Scanning Electron Microscopy (FESEM) with HITACHI SU8010 instrumentation (CIF LPU, India) together with Energy Dispersive Spectroscopy (EDS) elemental mapping facility. For particle size Ppy/TS0.2 NHs were also examined by TechnaiG^2 Transmission Electron Microscope (TEM) (SAIF AIIMS, New Delhi). Specific surface area, pore size and volume of the nanohybrids determined by Brunauer-Emmett-Teller (BET) surface study with N_2 adsorption and desorption with Quantachrome® ASiQwinTM- from Quantachrome Instruments.

Electrochemical characterizations

Electrochemical investigation was supported with Autolab Potentiostat/Galvanostat (PGSTAT 204, Netherland) advanced with NOVA 2.1 software. A three-electrode arrangement with graphite sheet (G) (working electrode), platinum wire (Pt) (counter electrode) and silver-silver chloride (Ag/AgCl) (reference electrode) was set up [5]. All photocatalysts were explored by using Electrochemical Impedance Spectroscopy in 1 M H_2SO_4 electrolyte to inspect their photelectric properties along with individual parameters.

Photocatalytic study

Experimental photocatalytic degradation of MB dye in aqueous solutions was carry out in direct solar light in a 250 mL conical flask. The photodegradation activities were achieved during May from 11:00 AM to 3:00 PM at DCRUST, Murthal, Sonepat (INDIA) (28.990 N; 77.022E). For each experiment, average solar light intensity was measured and found to be approximately 1.2×10^5 lx. For individual experiment, 1 mg of sample as photocatalyst to 10 parts per million (ppm) aqueous MB dye solution was taken in a 250 mL conical flask. Aqueous MB solution of optimized pH 8 with photocatalyst was then stirred for half an hour at room temperature in dark condition to achieve adsorption-desorption equilibrium. Initially, the pH of the suspension was set and did not regulate during the reaction. During solar light irradiation, 10 mL of suspensions were extracted after every 20 min time interval, then centrifugated to isolate the photocatalysts. Later, the supernatant was used for absorbance study by using UV-Visible spectrophotometer in

the range from 500 to 750 nm. Further, any drop out in major absorption peak was utilized to investigate photocatalysis effect in degradation of organic dye. The degradation efficiency during photocatalysis was calculated by using Eq. (1) [9],

$$E = \frac{C_o - C_t}{C_o} \times 100\% \quad (1)$$

where, C_o represents adsorption-desorption equilibrium concentration (mg/L) of solution at initial time ($t = 0$), C_t is solution concentration (mg/L) at a particular time ($t = 20$ to 120 min). The appreciable rate constant as predicted by adopting, the simplistic pseudo first order Langmuir-Hinshewood kinetic model of Eq. (2) [30],

$$\ln\left(\frac{C_o}{C_t}\right) = k_{app} \times t = kKt \quad (2)$$

where, t represents degradation time in min, C_o and C_t represents initial and final concentration of dye in mg/L, k_{app} represents apparent rate constant in min^{-1}, k is for reaction rate constant in min^{-1} and K is adsorption coefficient of dye onto photocatalyst particles surface.

Antibacterial study

The performance of synthesized Ppy/TS0.2 NHs was also examined for antibacterial activity in resistance to some pathogenic bacteria by using agar well diffusion method. All cultures utilized Staphylococcus. Aureus, Escherichia. coli, Klebsiella pneumoniae, and Shigella flexneri were obtained from Microbial Type Culture Collection (MTCC), Chandigarh. Protected media was produced then sanitized and at last, inoculated with pathogenic cultures (0.75 mL) after media got solidified. All wells were prepared for Ppy/TS0.2 NHs seeding with varying concentrations i.e., 10, 30, 50 and 70 µL ejected into each and individual well. Glass petri plates were then incubated at 37 ºC for 20 h in upstanding position and inhibition zones were spotted subsequently. All the tests were performed twice, and results were denoted as mean of ±0.01 in particular image. Further, bacterial inhibition tendency was investigated under solar irradiation for 150 min with and without NHs concentration in distinct bacterial culture.

Results and discussions

XRD spectral analysis

Figure 1 describes powder XRD patterns of neat Ppy, TS Nc and Ppy/TS NHs series over 2θ range of 10˚-80˚. XRD spectra of neat Ppy with distinctive peak at 26.16˚ designates its amorphous nature. The broadness of peak may be due to Vander-Waal interaction among polypyrrole chain as well counter ion interaction of pyrrole [31]. TiO_2-SiO_2 Nc and Ppy/TS NHs series also display broadened peak due to very less crystalline nature or small crystallite size of particles [32]. Polypyrrole doping in Ppy/TS NHs decreases the broadness of peak and shifts toward lower 2θ value. Further, very small increase in intensity is observed on increasing concentration of dopant from 0.1 to 0.3 g, which displays uniform dispersion of nanocomposites into the polymer matrix with decent interactions. Using Scherrer's equation, average crystallite size of Ppy, TS Nc and best Ppy/TS0.2 NHs is obtained to be approximately 30.01 nm, 13.32 and 18.37 nm, respectively also in good agreement with average size obtained by TEM histogram plot.

BET analysis

Nitrogen adsorption-desorption isotherms were achieved to obtain surface area, pore volume and pore size of nanohybrids at 77 K temperature. Figure 1b represents type II isotherm for Ppy/TS0.2 NHs, we presume that innumerous molecules of similar energy are captured into the polymer matrix voids [33]. A clear hysteresis loop in relative pressure ranging 0.35–0.85 indicated mesoporous nature of nanohybrids [34]. Figure 1c defines average multi-point BET adsorption plot with assessed specific surface area i.e., 56.41 m^2/g for NHs. The pore volume for NHs obtained to be 0.251 cm^3/g by pore volume BJH distribution plot. Figure 1d denotes pore size distribution by BJH method desorption [33]. Average pore diameter value for Ppy/TS0.2 NHs obtained to be 1.185 nm. BET study evidently displayed mesoporous nature of nanohybrids with improved surface area.

UV-Vis spectral study

Figure 2a denotes the UV-Vis absorption spectrum of Ppy, TiO_2-SiO_2 Nc and Ppy/TS NHs series calcinated at 500 ^oC from 200 to 800 nm range. The inset plot shows UV-Vis spectrum of TS Nc with its precursors. Clearly, the absorbance band of TS Nc is at higher wavelength as compared to the precursors. The red shift in absorbance band pointed towards formation of charge transfer complexes [21]. For Ppy, the absorbance is very small in whole region with a weak absorbance peak between 400 and 500 nm and a strong peak between 200 and 300 nm. Though, below 250 nm the absorbance of Ppy increased gradually with decrease in wavelength and displayed a broad absorbance band at 286 nm [35]. The wavelength range denoted л*→л type electronic transitions associated with Ppy [29]. Further, Ppy doping in Ppy/TS NHs series again shifted the

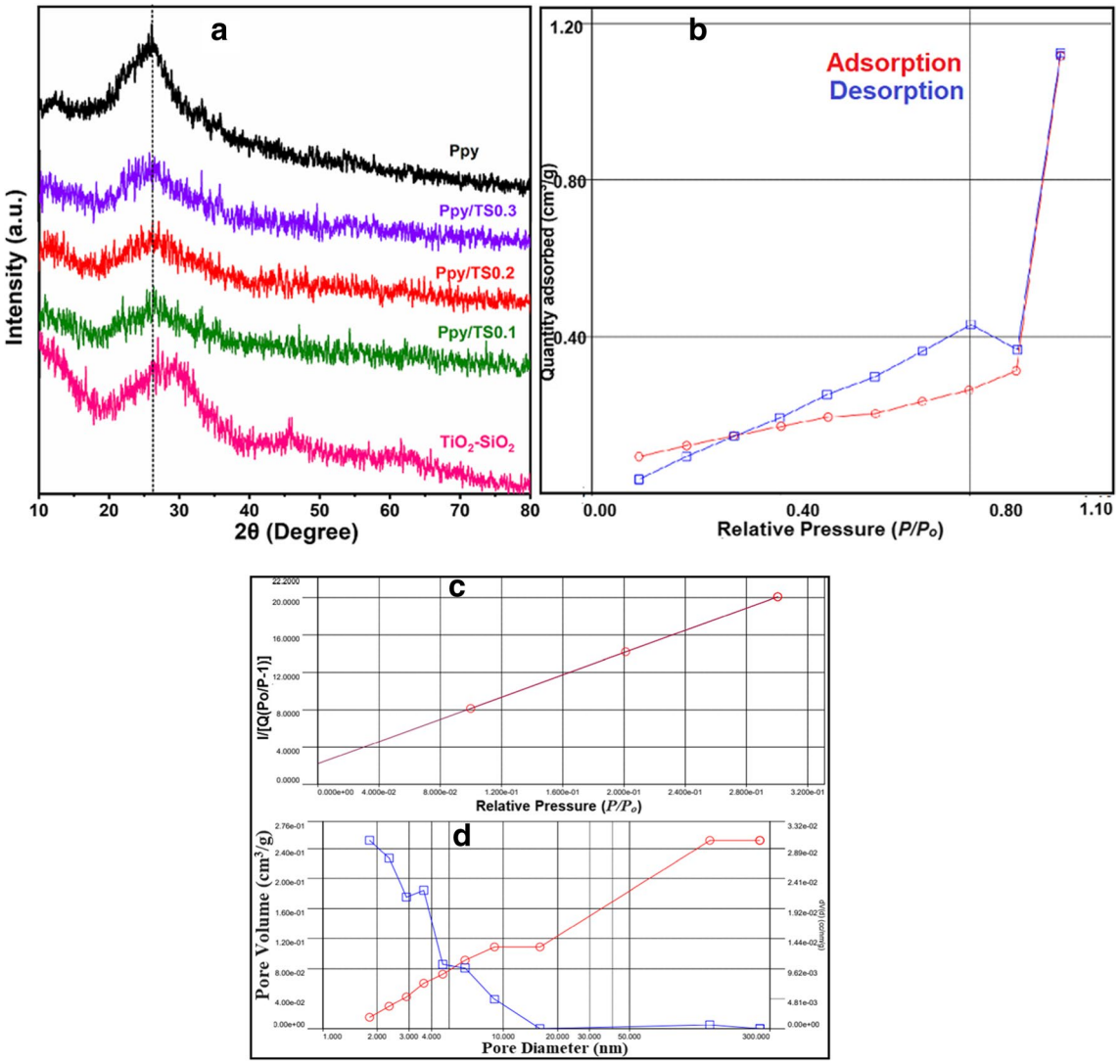

Fig. 1 **a** XRD of TS Nc, Ppy/TS NHs series and neat Ppy **b** Nitrogen absorption-desorption isotherm Ppy/TS0.2 NHs **c** Specific surface area plot and **d** BJH method differential plot for pore diameter

absorption band toward higher wavelength and increased absorbance. But for Ppy/TS0.2 NHs, the absorption spectra showed highest absorbance and larger red shift in comparison to Ppy/TS0.3 NHs [3]. Figure 2b represents Tauc's plot by using Davis and Mott relation of direct transition $((\alpha h\nu)^2 = B(h\nu - E_g))$, here α represents coefficient of absorption, E_g is band gap and B, a constant value. Band gap is calculated by generalizing the linear segment of curve to absorption equal to zero [6]. The inset plot depicts the band energy plot for TiO_2, SiO_2 and TiO_2-SiO_2 Nc with band gap values, 4.31 eV, 3.38 eV and 3.34 eV, respectively. Whilwe the band gap values for neat Ppy Ppy/TS0.1 NHs, Ppy/TS0.2 NHs and Ppy/TS0.3 NHs are calculated to be 4.25 eV, 3.67 eV, 3.26 eV and 3.51 eV, respectively. We observed that our best Ppy/TS0.2 NHs exhibited lowest band gap with highest charge transfer tendency.

XPS spectral analysis

Figure 3a represents the XPS spectra of TiO_2-SiO_2 Nc and Ppy/TS0.2 NHs with elemental composition of nanomaterials. The spectrum clearly exhibited the valence shell of C, N, O, Ti, and Si elements. Figure 3b denotes high resolution C1s spectrum of Ppy doped TiO_2-SiO_2 Nc with three binding energy peaks at 281.7 eV for C-H and C-N bonds, 283.2 eV for C-C, C-O-Ti bonds and 285.6 eV for C = C and C = O bonds [36]. Figure 3c depicts the XPS spectrum of N1s with two peaks at 399.2 eV for N-H bond and 407.1 eV for C-N bond in Ppy matrix. Figure 3d shows core level spectrum of O1s for TiO_2-SiO_2 Nc, ascribed for binding energy peaks at 527.2 eV, 528.5 eV and 530.1 eV for Ti-OH, Si-OH and Ti-O bonds, respectively [21]. For Ppy/TS0.2 NHs, the binding energy peaks shifted to higher values i.e., 528.9 eV,

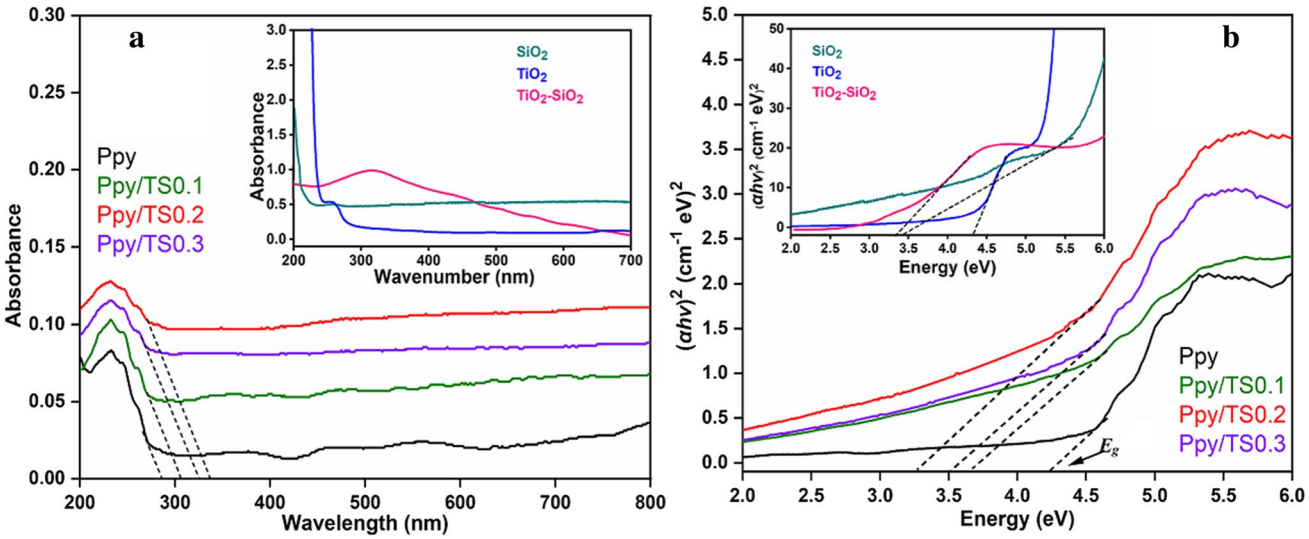

Fig. 2 **a** absorbance spectra and **b** Tauc's plots of Ppy, TS Nc and Ppy/TS NHs series, respectively

530.2 eV and 530.4 eV, respectively. The spectra evidenced the presence of O^{2-} ions at the nanohybrids surface [37]. Figure 3e displays core level XPS spectra of Ti2p for TS Nc and Ppy/TS0.2 NHs with two absorption peaks. The two binding energy peaks at values 461.6 eV and 455.8 eV are attributed to $Ti2p_{1/2}$ to $Ti2p_{3/2}$ spin-orbital splitting and shifted to higher value for Ppy/TS0.2 NHs (Fig. 3e). The binding energy difference i.e., 5.8 eV in these peaks clearly confirmed existence of Ti^{+4} and Ti^{+3} ions in TiO_2 already defined in few reports(Yadav et al. 2022). Figure 3f designates the XPS spectrum of Si 2p for TS Nc unveiled a peak at 99.8 eV conforming presence of Si^{+4} ions in amorphous silica and reduced to binding energy value of 99.1 eV for Ppy/TS0.2 NHs [38]. Thus, XPS results confirmed the doping of Ppy with proper interaction in nanohybrid formation.

FESEM and EDS study

FESEM images of Ppy, TiO_2-SiO_2 Nc and Ppy/TS0.2 NHs are shown in Fig. 4a-c, respectively at 20kx magnification. Neat Ppy shows spherical morphology at 20kx scale with consistent size dispersal [31]. SEM image of TS Nc displays irregular shaped structures at same scale [21]. Figure 4c clearly displays the regular distribution of TS Nc in spherical shaped PPy matrix forming globular morphological view. Figure 4d portrays EDS spectrum of Ppy/TS0.2 The EDS pattern of NHs indicates the existence of particular peaks with equivalent wt % of elements C, O, N, Ti and Si and respectively. Moreover, detection of no other element authenticates the purity and formation of nanohybrids.

TEM analysis

Figure 5 represents TEM micrographs of TS nanocomposites and Ppy/TS0.2 NHs, respectively at same scale. TEM micrograph of sol-gel produced TS Nc with an average particle size of 13.37 nm is shown in Fig. 5a at 100 nm scale. We can perceive that mesoporous silica is enclosed by unevenly spread spherical anatase TiO_2 nanoparticles in TS Nc evidently with accumulation. Figure 5b denotes TEM micrograph of best sample Ppy/TS0.2 NHs at 100 nm scale. It displays consistent distribution of nanocomposites in Ppy matrix to form Ppy/TS NHs. Figure 5c represents size distribution histogram plot of Ppy/TS0.2 NHs with an average grain size of 32.54 nm.

EIS analysis

Electrochemical impedance spectra were adopted to observe interfacial properties of TiO_2-SiO_2 Nc along with its precursors, neat Ppy and Ppy/TS NHs formed after doping by evaluating frequency and resistance behavior of all. EIS study was achieved in frequency range 10^5-0.1 Hz to explore electron transfer tendency of modified electrode after nanomaterials coating in electrolyte solution. The modified graphite sheet electrodes were used. Figure 6a shows Nyquist plots of Ppy, Ppy/TS0.1, Ppy/TS0.2 and Ppy/TS0.3 HMs along with TS Nc and its precursors in inset plot. In Nyquist plots, - Z" and Z' denotes imaginary and real impedance, respectively. All modified electrode materials displayed approximately vertical line with no semicircular section clarified minimum charge storage movement.

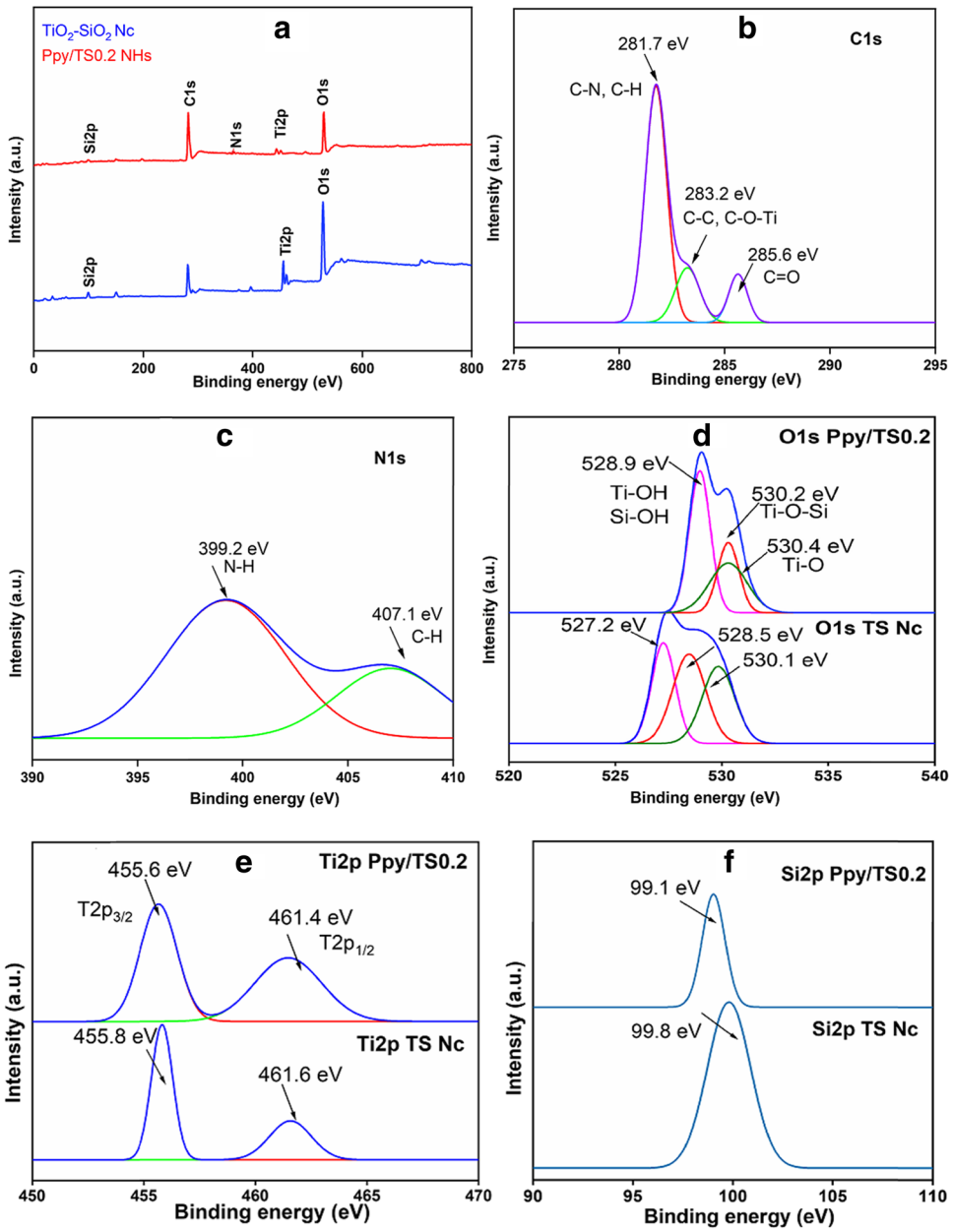

Fig. 3 **a** XPS binding energy spectra of TiO_2-SiO_2 Nc and Ppy/TS0.2 NHs and corresponding high-resolution spectra's for **b** C 1s **c** N 1s **d** O 1s **e** Ti 2p and **f** Si 2p

The electrical equivalent circuit is fitted to experimental statistics to analyze Nyquist plot intensely. Figure 6b denotes experimental and fitted data for Ppy/TS0.2 sample with equivalent simulated EEC as inset. EEC circuit represents "R_s" for electrolyte or solution resistance, "R_{ct}" for charge transfer resistance, "CPE" for constant phase element and C_{dl} for capacitance. The EEC fitted data of EIS for Ppy, TS Nc and Ppy/TS NHs series is represented by Table 1. The best sample Ppy/TS0.2 NHs showed lowest R_s and R_{ct} values i.e., 0.66 Ω and 0.235 Ω, respectively as compared to rest of the samples. Even the n value for Ppy/TS0.2 NHs is 0.85 which is near to 1 also describes their capacitive view. Thus, Ppy/TS0.2 NHs performed as rapid charge transfer complexes during photocatalytic reactions [9].

Photocatalytic activity

The doping effect of Ppy in TS Nc was inspected for degradation of methylene blue dye in aqueous solution of pH 8. Figure 7a-f represents UV-Visible absorbance spectra for MB dye in presence of all precursors, nanocomposites and nanohybrids with variation in contact time. It is observed that TS Nc showed better degradation in comparison to TiO_2 and SiO_2 precursors. Further, after Ppy doping the nanohybrid series i.e., Ppy/TS0.1, Ppy/TS0.2 and Ppy/TS0.3 exhibited enhanced photodegradation than TS Nc alone. Ppy/TS0.1 NHs showed degradation efficiency value 75.16% which further increased with Ppy doping. Ppy/TS0.2 NHs revealed highest degradation efficiency with value 90.48%. The photocatalytic activity was found in order of

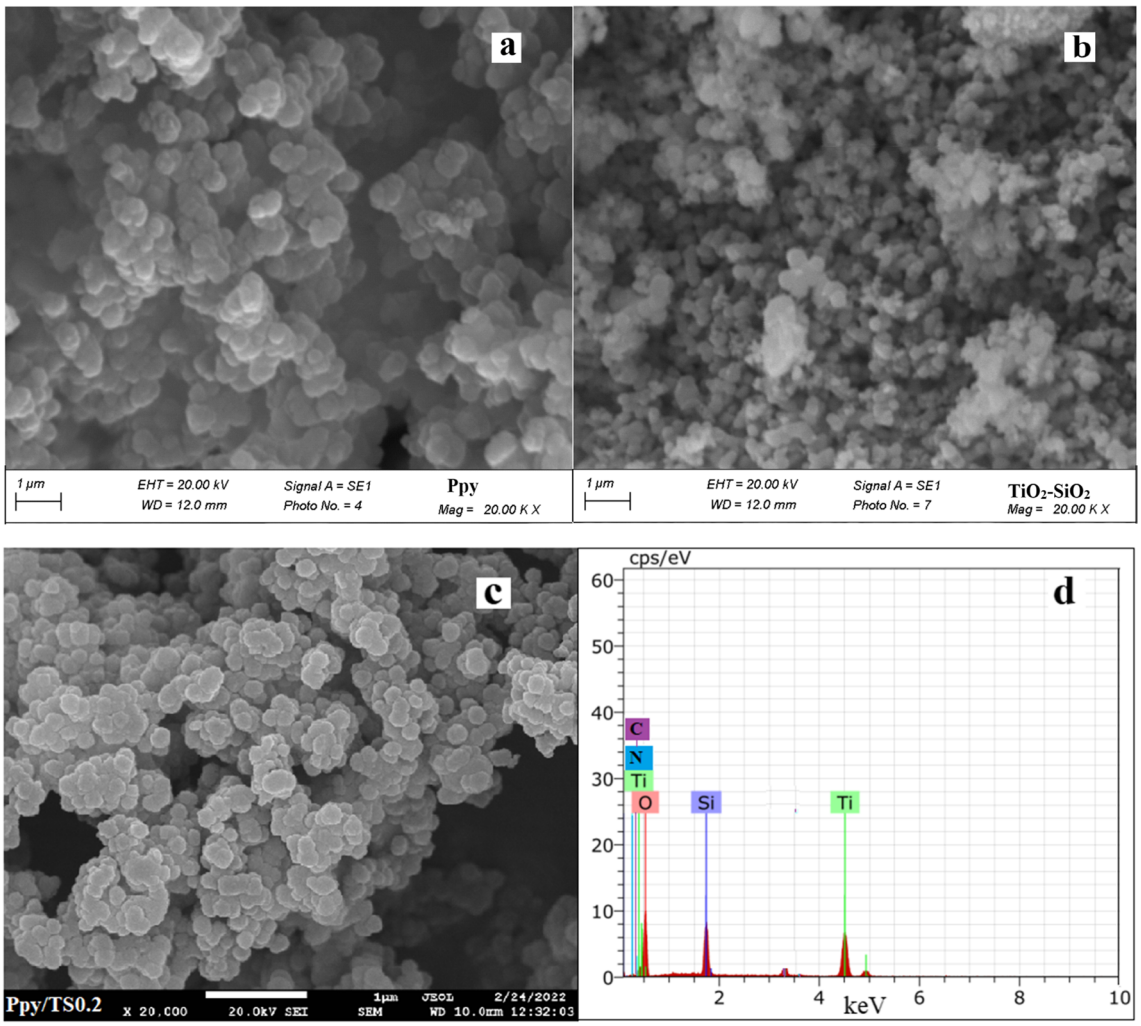

Fig. 4 SEM images of **a** Ppy **b** TiO_2-SiO_2 Nc and FESEM image of **c** Ppy/TS0.2 NHsand **d** EDS of Ppy/TS0.2 NHs

$SiO_2 < TiO_2 <$ TS Nc < Ppy/TS0.3 NHs < Ppy/TS0.1 NHs < Ppy/TS0.2 NHs. The decreased activity of Ppy/TS0.3 NHs in comparison to Ppy/TS0.2 NHs could be due to hinderance in NHs and thus recombination of e^-h^+ pairs by increased Ppy concentration. Prior to photodegradation, MB dye suspensions were kept in dark for 30 min. During decolorization processes in dark adsorption, no significant change in MB percentage was noticed. Figure 8a, b represents the degradation efficiency (%) and apparent rate constant ($_{kapp}$) for MB dye degradation over a period of 120 min and also summarized in Table 2. The higher degradation tendency of NHs may be due to synergic effect between nanocomposites and Ppy [39]. Additionally, mineralization degree of antibiotics was determined by using total organic carbon (TOC). Figure 8c represents TOC removal % in various antibiotics. It was observed that Ppy/TS0.2 NHs exhibited highest (90.48%) TOC removal efficiency at optimum conditions (Initial concentration = 100 mg/L, Catalyst loaded = 10 mg/L, pH = 8, Time = 120 min). Further, the photocatalytic degradation capability of our best Ppy/TS0.2 nanohybrid is compared with some pre reported work toward MB dye in Table 3.

Effect of pH of solution

The pH of solution is an important parameter that contribute towards degradation of MB dye by dictating surface charge of photocatalyst and size of aggregate formed. Ppy/TS0.2 NHs showing best degradation rate was further investigated against different pH of dye solution with photocatalyst. Figure 8d clearly shows degradation efficiency increases as pH of MB dye solution increases. As per the reports MB dye shows increased degradation rates at higher pH due to strong adsorption of dye onto catalyst surface [30]. At low pH, the photocatalyst NHs acted as cationic species and considered week adsorption of cationic MB dye onto catalyst surface.

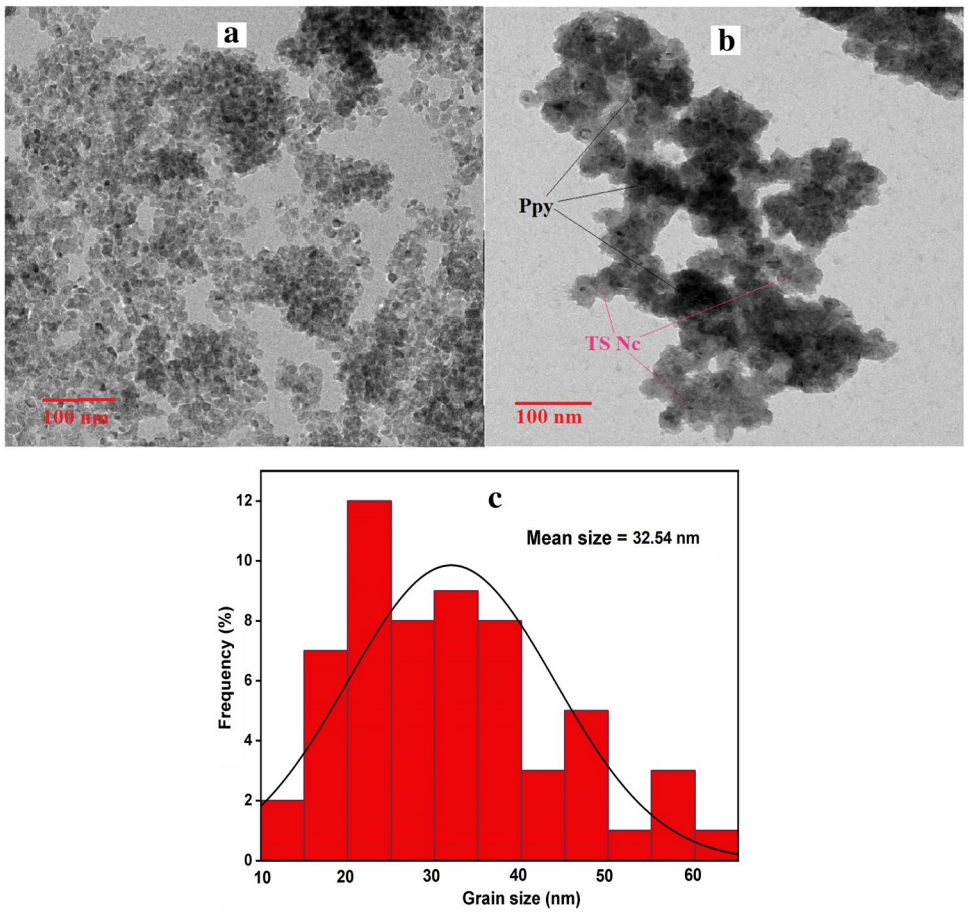

Fig. 5 TEM images of **a** TS Nc **b** Ppy/TS0.2 NHs at 100 nm scale **c** histogram plot for Ppy/TS0.2 NHs

Further, on increasing pH up to 8, NHs acted as anionic species and thereby enhanced adsorption of dye. Moreover, increase in pH afterwards, the $OH^{\bullet-}$ radicals scavenged quickly prior to react with dye and thereby decreased degradation rates [43]. So, the optimized pH for MB dye solution with catalyst is found to be 8. The inset plot displays Zeta

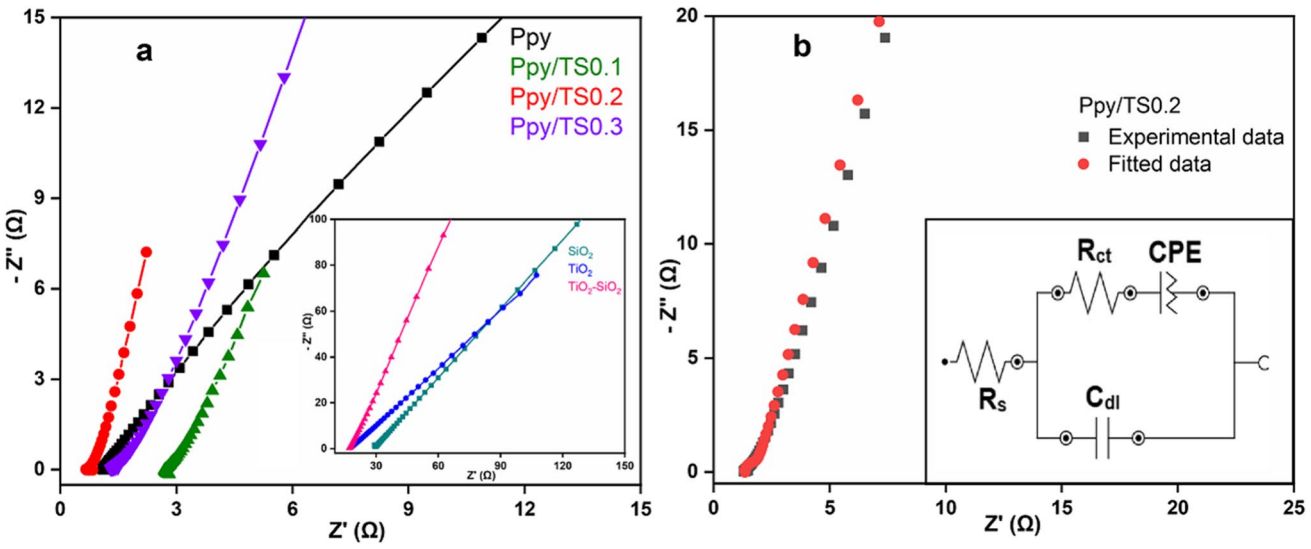

Fig. 6 Nyquist plots of **a** Ppy and Ppy/TS NHs series, Inset: TiO_2, SiO_2 and TS Nc **b** Fitted and experimental data for Ppy/TS0.2 NHs with equivalent electrical circuit

Table 1 EEC fitted data of EIS for different samples

Sample	R_S (Ω)	R_{ct} (Ω)	CPE (mMHO)	*n*	C_{dl} (mF)
TiO_2	17.2	1.67	10.1	0.53	25.6
SiO_2	29.41	2.27	4.26	0.49	29.7
TiO_2-SiO_2	16.96	1.18	18.0	0.58	6.84
Ppy/TS0.1	2.73	0.413	184	0.75	29.5
Ppy/TS0.2	0.66	0.235	172	0.85	26.3
Ppy/TS0.3	1.26	0.809	270	0.73	91.2
Ppy	1.09	2.14	12.2	0.48	1.05

potential (mV) of Ppy/TS0.2 NHs in MB dye solution of pH 8. The pH_{PZC} value of above suspension is found to be 6.58.

To examine the consequences due to active species in MB dye degradation rate, trapping tests using organic/inorganic quenching agents were performed. Figure 9a represents the photodegradation of MB with $K_2Cr_2O_7$, Methanol, Ascorbic acid (AA) and NaN_3 quenchers. They were adopted as free radicals, electrons, and holes scavengers, respectively for MB photodegradation using UV-Vis spectrophotometer after 120 min solar irradiation [3, 44]. $K_2Cr_2O_7$ showed very less hinderance and higher degradation while NaN_3 exhibited least degradation rate due to higher quenching of superoxide radical.

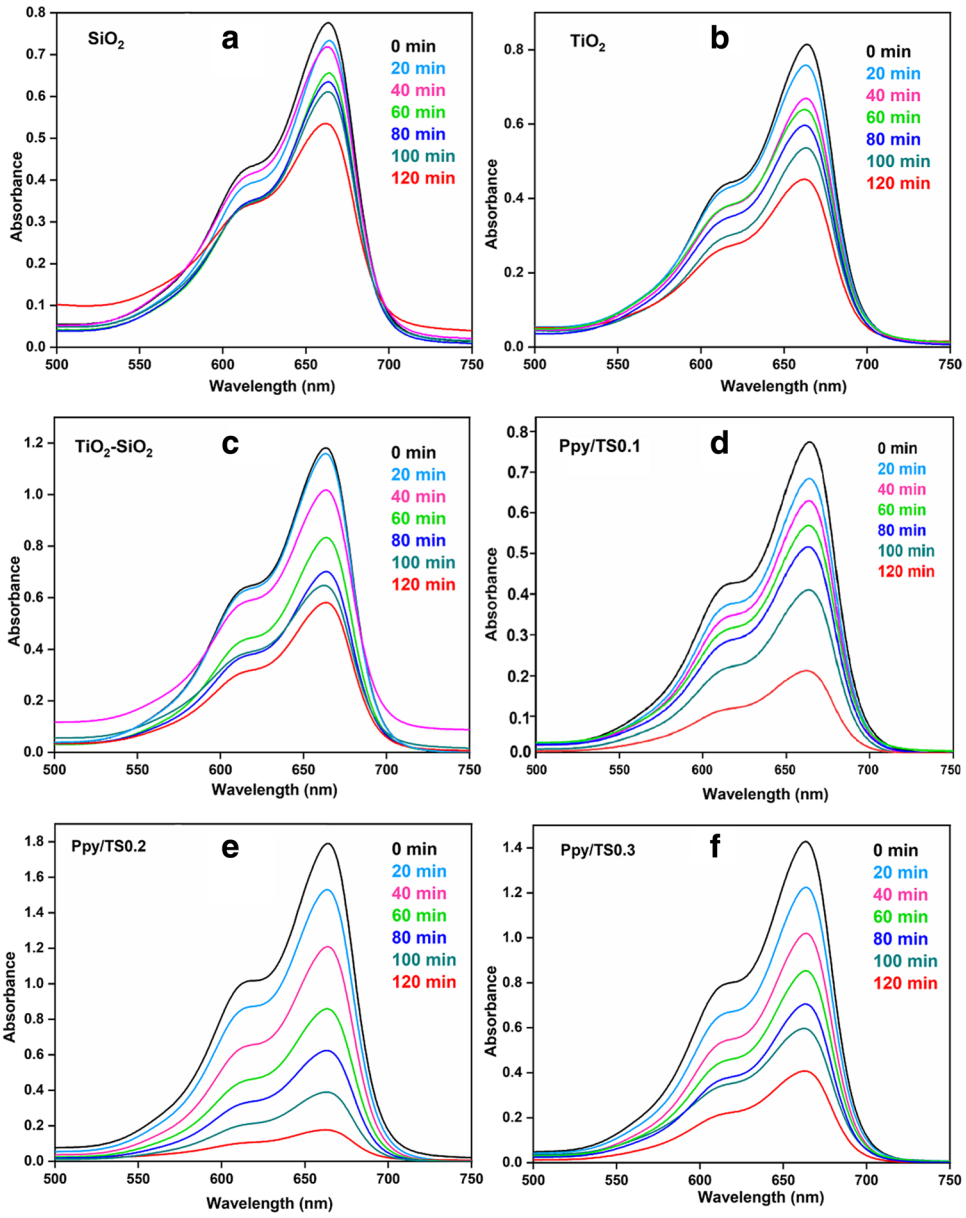

Fig. 7 UV-Vis degradation spectra of MB dye (pH 8) in solar irradiation using precursors, TS Nc and Ppy/TS NHs series photocatalysts

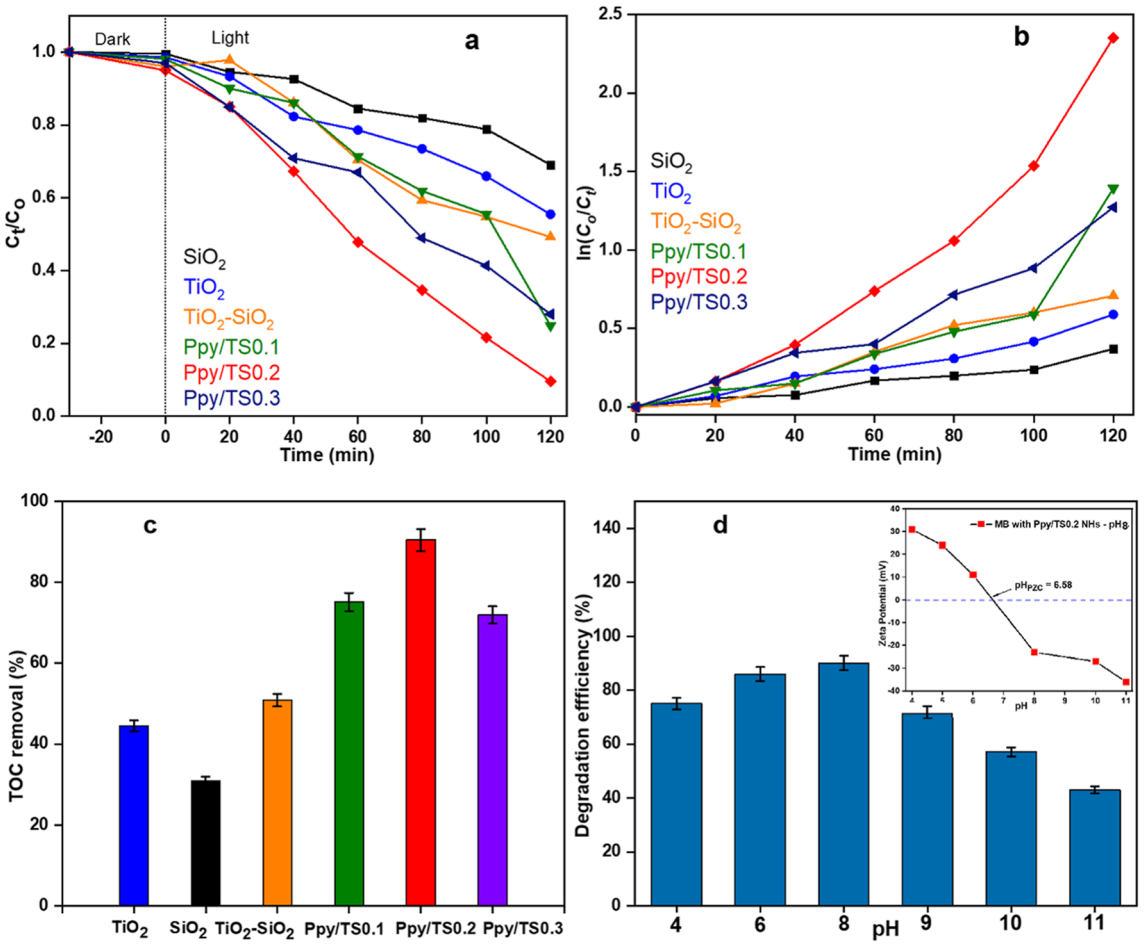

Fig. 8 **a** Photocatalytic activity comparison towards MB dye degradation **b** $\ln(C_0/C_t)$ for dye degradation as function of simulated solar irradiation time **c** TOC % removal in various systems and **d** Degradation efficiency of MB dye at various pH; Inset: Zeta potential vs. pH of dye solution with Ppy/TS0.2 NHs photocatalyst

Figure 9b shows recyclability and reusability study of Ppy/TS0.2 NHs sample upto four cycle runs. The catalyst was collected at the end of each cycle and reused in similar conditions upto four runs. A slight decrease in photodegradation was observed at the end of last cycle that may be due to loss of negligible amount of photocatalyst during recovery.

Table 2 Degradation efficiency with apparent rate constant for TiO_2-SiO_2 Nc, their precursors, and Ppy/TS NHs series toward photocatalytic degradation reaction of MB dye for t = 120 min

S. No. constant (k_{app})	Sample (min^{-1})	Degradation efficiency (%)	Apparent rate
1.	TiO_2NPs	44.53	0.0049
2.	SiO_2 NPs	30.97	0.0031
3.	TiO_2-SiO_2 N_C	50.81	0.0059
4.	Ppy/TS0.1 NHs	75.16	0.0116
5.	Ppy/TS0.2 NHs	90.48	0.0196
6.	Ppy/TS0.3 NHs	71.97	0.0106

Antimicrobial study of nanohybrids

The results for antibacterial study against the bacteria are encapsulated in Fig. 10a. Ppy/TS0.2 NHs showed highest percentage inhibition efficiency for E. coli followed by S. aureus, S. flexneri and K. pneumoniae with an inhibitory concentration of 70 µL. The results clearly displayed inhibition zones variation from 9 to 27 mm range in diameters for Ppy/TS0.2 NHs. Figure 10b showed that increase in concentration of Ppy/TS0.2 NHs from 10 to 70 µL, enhanced the antibacterial efficiency for all bacteria. Further, the antimicrobial efficacy was investigated with solar irradiation as control for different bacteria in absence and presence of 70 µL of Ppy/TS0.2 NHs concentration. As per the results shown in Fig. 10c, the solar irradiation without any NHs concentration revealed quite

Table 3 Comparison of Ppy/TS0.2 NHs photocatalyst for photocatalytic MB dye degradation with similar previous reports

Material used	Illumination Source	Conc. of Catalyst (g/L)	Dye solution Conc. (mg/L)	Degradation time (min)	Degradation efficiency (%)	References
CdSe-rGO NH	Hg lamp 8 W	0.375	10	210	70	[40]
Ag doped g-C_3N_4	Xe lamp 200 W	0.1	10	120	96	[10]
GCN-Ag1NC	Tungsten lamp 200 W	0.1	10	120	96	[41]
g-C_3N_4	Xe lamp 200 W	0.1	10	60	60	[30]
Ag/ZnO NC	Tungsten lamp 200 W	0.1	10	120	94.27	[9]
GCN-ZnO	Tungsten lamp 200 W	0.1	10	80	78	[3]
ZnO/CdO	Halogen lamp 250 W	0.01	10	120	30	[42]
Ppy/TS NHs	Solar light 1.2×10^5 lx	0.02	10	120	90.48	Present work

poor inactivation rate even after 150 min irradiation time. From the reports, lower temperatures (> 40 ˚C) affect the antibacterial rate negligibly and temperature greater than 45 ˚C show appreciable bacterial inhibition [45]. While under solar irradiation with NHs concentration exposed improved inhibition efficiency against all bacteria attributable to synergic effect in photocatalysis. Besides the toxicity of Ti^{+4} species, the photo-induced reactive oxygen species (ROS) by TiO_2-SiO_2 Nc enhanced the antimicrobial activity [46]. Such antibacterial analysis for variety of bacteria have already been deliberated using discrete polymeric-metal oxide-based nanocomposites and similar composite materials [47–51].

Proposed mechanism

The proposed mechanism for antimicrobial study is represented by Fig. 11a. The proposed mechanism for antibacterial study is that the metal cations (Ti^{+4}) react with negatively charged bacterial cell and lead to cell damage either by deactivating protein, damaging DNA, hindering electron transport, or varying membrane permeability [52]. To determine the possible interaction mechanism between NHs and UV, position of both conduction and valence bands (E_{CB} *and* E_{VB}) were obtained by using Mulliken electronegativity theory equations [53].

$$E_{CB} = \chi - E_C - 0.5E_g \tag{3}$$

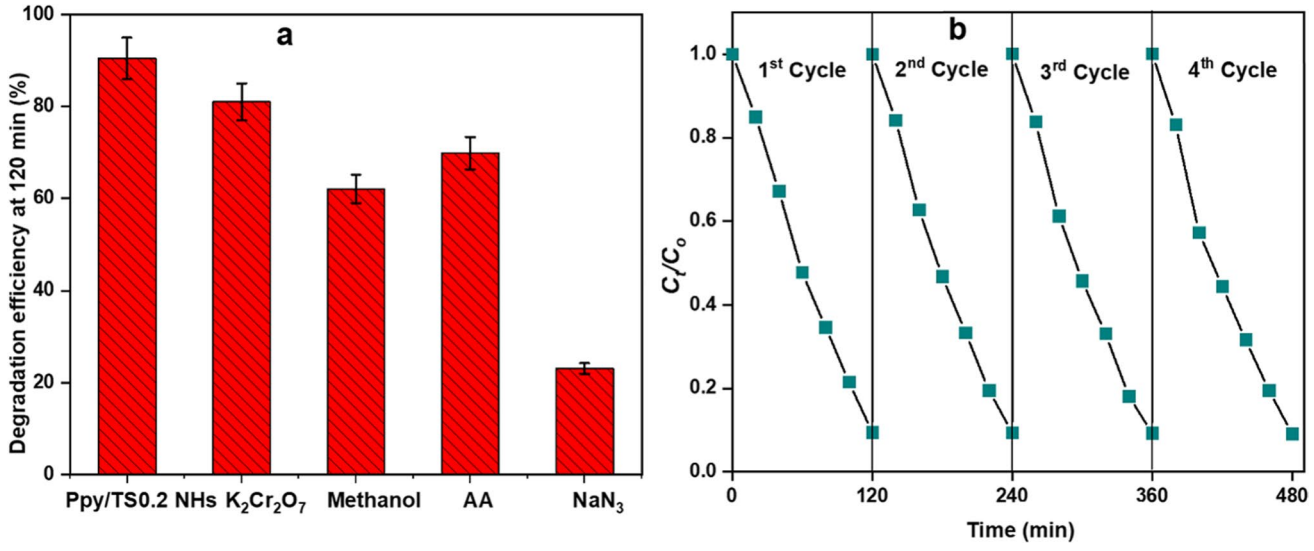

Fig. 9 **a** Influence of scavengers on MB dye degradation after 120 min solar irradiation **b** Recyclability study of MB dye degradation with photocatalyst Ppy/TS0.2 NHs in solar irradiation

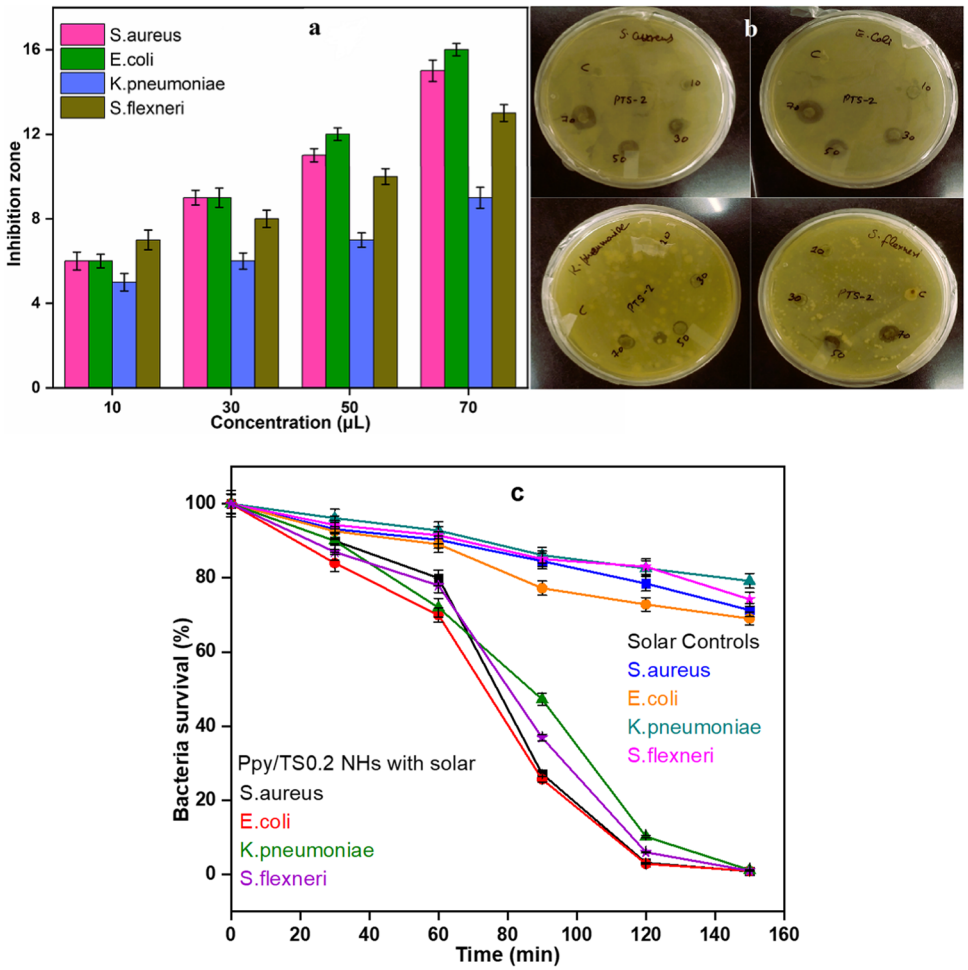

Fig. 10 **a** Comparative inhibition zones of NCs against distinct bacteria **b** Inhibition zones by agar diffusion method and **c** Antimicrobial activity with solar irradiation without and with Ppy/TS0.2 NHs (70 µL) in opposition to E. coli, K. pneumoniae, S. aureus and S. flexneri

$$E_{VB} = E_{CB} + E_g \quad (4)$$

Where χ is Mulliken electronegativity constant, E_{CB} *and* E_{VB} are potentials of semiconductor bands, E_c is free electrons energy ≀ 4.5 eV) on normal hydrogen scale and E_g is band gap energy of material. Under UV light NHs are excited to form photogenerated $e^{-}h^{+}$ pairs. Nanomaterials can also behave as photocatalysts by producing reactive oxygen species (ROS) i.e., superoxide, hydroxyl and H_2O_2 radicals with dissolved oxygen [45]. Figure 11b denotes the proposed mechanism for improved photocatalytic degradation potential. As we have observed that Ppy/TS NHs

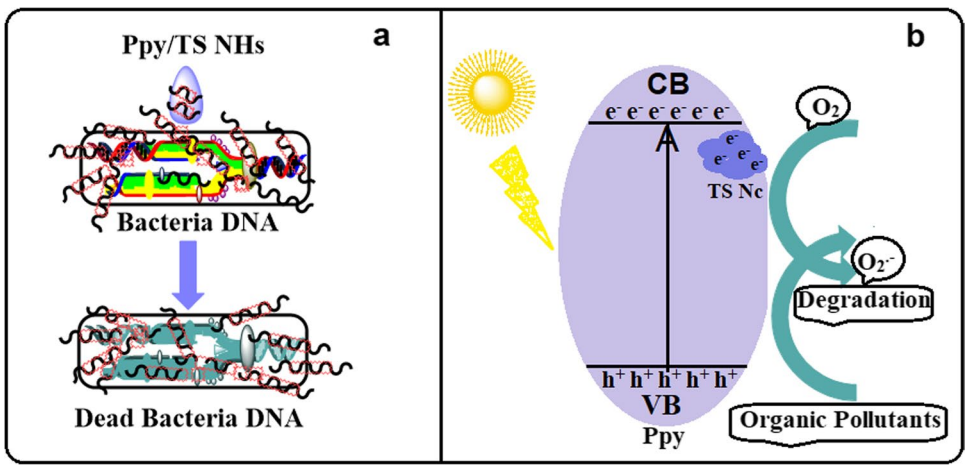

Fig. 11 Proposed mechanism for **a** antimicrobial and **b** photocatalytic showing separation and transfer of photogenerated electron-hole pairs over Ppy/TS NHs under solar irradiation

series showed increased dye degradation tendency than the nanocomposites and pure samples [54, 55]. This behaviour leads to increased visible light absorption capability along with reduced band gap on increasing amount of dopant Ppy. From Fig. 11b we can see when visible light falls onto nanohybrid surface, valance band electrons get excited by absorbing light and move toward conduction band, thus by creating holes in valance band [41]. These electrons generate superoxide ($O_2^{\bullet-}$) radicals by combining with oxygen and these radicals can photodegrade the organic pollutants easily.

Conclusion

Polypyrrole doped TiO_2-SiO_2 nanohybrids (Ppy/TS NHs) series was synthesized thru in-situ oxidation polymerization by increasing weight ratio of pyrrole. The formation of NHs was authenticated by spectroscopical and morphological characterizations. The electron transport tendency of synthesized Ppy/TS0.2 NHs investigated by EIS analysis was found to be highest. The nanohybrids and precursors were examined for photocatalytic degradation of MB dye and revealed enhanced degradation tendency for the NHs series photocatalysts. It was observed that pyrrole doping (0.1 to 0.3 g) to TS Nc improved the photocatalytic ability of NHs series. The maximum photodegradation efficiency was found to be 90.48% in 120 min for Ppy/TS0.2 NHs under direct solar light. Additionally, Ppy/TS0.2 NHs performed significantly toward antimicrobial studies against some Gram-positive and Gram-negative deleterious bacteria, Escherichia coli, Klebsiella pneumoniae, Staphylococcus aureus, Shigella flexneri microbes.

Author contributions All authors contributed to study conception and design.

Meena Yadav Conceptualization; Data curation; Funding acquisition; Investigation; Methodology; Resources; Validation; Roles/Writing - original draft.

Rajat Arora Formal analysis, Data curation, Resources.

Monika Dhanda Formal analysis, Data curation, Resources.

Simran Ahlawat Formal analysis, Data curation, Resources.

Sachin Shoran Photocatalytic degradation analysis resources and Formal analysis.

Suman Ahlawat Formal Analysis, Data Curation, Visualization.

S. P. NehraPhotocatalytic degradation analysis resources, Formal analysis and Investigation.

Geeta Singh Supervision; Formal analysis, Investigation, Validation; Visualization; Writing - review and editing.

Suman Lata Conceptualization; Supervision; Methodology; Formal analysis, Investigation, Validation; Visualization; Writing - review and editing.

Funding The authors are obligated to Council of Scientific and Industrial Research, New Delhi, India for awarding fellowship to Meena Yadav (award letter no. 09/1063(0028)/2019-EMR-I), University Grant Commission (UGC), Delhi for providing fellowship to Monika Dhanda as JRF. (Ref. No. 201610158088) and Deenbandhu Chhotu Ram University of Science and Technology, Murthal for providing University Research Scholarship to Rajat Arora (Endst. No. DCRUST/Sch./2019/508) and Simran Ahlawat (Endst. No. DCRUST/Sch./2021/218–223).

Data availability Supplementary data and material will be published as received from the author.

Declarations

Ethical approval The research submitted is carried out in compliance with relevant institutional biosafety and biosecurity protocols.

Consent to participate Informed consent was obtained from all individual participants included in the study.

Consent to publish The authors affirm that participants provided informed consent for publication of all images in Figures.

Competing interests The authors declare no conflict of interest.

References

1. Liang R, Du Y, Xiao P, Cheng J, Yuan S, Chen Y, et al. Transition metal oxide electrode materials for supercapacitors: a review of recent developments. Nanomaterials. 2021;11(5):1248.
2. Yadav M, Singh G, Lata S. Revisiting some recently developed conducting Polymer@Metal oxide nanostructures for electrochemical sensing of vital biomolecules: a review. J Anal Test. 2022;6(3):274–295.
3. Paul DR, Gautam S, Panchal P, Nehra SP, Choudhary P, Sharma A. ZnO-Modified g-C3N4: a potential photocatalyst for environmental application. ACS Omega. 2020;5:3828–38
4. Kavuri HA, Kihara S, McGillivray DJ, Willmott G. Poly(vinyl pyrrolidone)-modified metal oxide anode interlayers for stable organic solar cells. J Photon Energy. 2020;10:1.
5. Dhanda M, Nehra SP, Lata S. The amalgamation of g-C3N4 and VO2 (D) as a facile electrode for enhanced storage of energy. Synth Met [Internet]. 2022;286:117046. Available from: https://linkinghub.elsevier.com/retrieve/pii/S0379677922000406. Accessed May 2022.
6. Yadav M, Singh G, Lata S. Sol–gel-assisted synthesis of PVPO-TiO2 nanocomposites extended to bifunctionality as efficient electrode for enzymeless D-(+)-glucose sensing and antimicrobial potential. J Solid State Electrochem [Internet]. 2022. https://doi.org/10.1007/s10008-022-05216-9
7. Pahuja P, Malik R, Saini N, Kumar S, Lata S. PPy–TiO2–phenylalanine composites as anticorrosive coatings electrodeposited over Fe–C steel surface in the marine environment. J Adhes Sci Technol. 2020;34:1823–39.
8. Yadav M, Singh G, Lata S. Polyvinylpyrrolidone/TiO2 composites' preparation via sol–gel procedure furthered with non-enzymatic glucose sensing and antibacterial effectiveness. Environ Sci Pollut Res [Internet]. 2022. https://doi.org/10.1007/s11356-022-21558-3
9. Panchal P, Paul DR, Sharma A, Choudhary P, Meena P, Nehra SP. Biogenic mediated Ag/ZnO nanocomposites for photocatalytic and antibacterial activities towards disinfection of water. J Colloid Interface Sci. 2020;563:370–80.
10. Paul DR, Sharma R, Panchal P, Malik R, Sharma A, Tomer VK, et al. Silver doped graphitic carbon nitride for the enhanced

photocatalytic activity towards organic dyes. J Nanosci Nanotechnol. 2019;19:5241–8.
11. Kamalvandi P, Akhlaghian F. Copper cable doped with tin oxide and its application to photodegrade natural organic matters. J Environ Health Sci Eng. 2022;20:555–63.
12. Pandey G, Singh S, Hitkari G. Synthesis and characterization of polyvinyl pyrrolidone (PVP) coated Fe 3 O 4 nanoparticles by chemical co precipitation method and removal of Congo red dye by adsorption process. Int Nano Lett [Internet]. Springer, Berlin Heidelberg; 2018; Available from: https://doi.org/10.1007/s40089-018-0234-6
13. Khannyra S, Luna M, Gil MLA, Addou M, Mosquera MJ. Self-cleaning durability assessment of TiO2/SiO2 photocatalysts coated concrete: effect of indoor and outdoor conditions on the photocatalytic activity. Build Environ. 2022;211:108743.
14. Temerov F, Haapanen J, Mäkelä JM, Saarinen JJ. Photocatalytic activity of multicompound tio2 /sio2 nanoparticles. Inorganics (Basel). 2021;9(4):21.
15. Panchal P, Paul DR, Sharma A, Hooda D, Yadav R, Meena P, et al. Phytoextract mediated ZnO/MgO nanocomposites for photocatalytic and antibacterial activities. J Photochem Photobiol A Chem. 2019;385:112049.
16. Sharifi-Bonab M, Aber S, Salari D, Khodam F. Synthesis of CoZnAl-layered double hydroxide/graphene oxide nanocomposite for the removal of methylene blue: kinetic, thermodynamic, and isotherm studies. Environ Prog Sustain Energy. 2020;39:e13316.
17. Badry R, Ibrahim A, Gamal F, Shehata D, Ezzat H, Elhaes H, et al. Electronic properties of polyvinyl alcohol/ TiO2/SiO2 nanocomposites. Biointerface Res Appl Chem. 2020;10:6427–35.
18. Pazhamalai P, Krishnamoorthy K, Mariappan VK, Kim SJ. Blue TiO2 nanosheets as a high-performance electrode material for supercapacitors. J Colloid Interface Sci. 2019; 536:62–70.
19. Fu L, Zheng YH, Fu ZX. Ascorbic acid amperometric sensor using a graphene-wrapped hierarchical TiO2 nanocomposite. Chem Pap. 2015;69(5):655–61.
20. Sun S, Deng T, Ding H, Chen Y, Chen W. Preparation of nano-TiO2-coated SiO2 microsphere composite material and evaluation of its self-cleaning property. Nanomaterials. 2017;7(11):367.
21. Yadav M, Dhanda M, Arora R, Jagdish R, Singh G, Lata S. Titania (TiO_2)/silica (SiO_2) nanospheres or NSs amalgamated on a pencil graphite electrode to sense < scp > l -ascorbic acid electrochemically and augmented NSs for antimicrobial behaviour. New J Chem [Internet]. 2022. Available from: http://xlink.rsc.org/?DOI=D2NJ01892F. Accessed 06 Jun 2022.
22. Babu AT, Antony R. Binary metal oxide nanocomposites of Fe, Co and Mn with SnO2 for photodegradation of dyes, catalytic reduction of 4-nitrophenol and antimicrobial activities. React Kinet Mechan Catal. 2022;135:539–53.
23. Saini N, Kuma R, Pahuja P, Malik R, Malik R, Singhal S, et al. Exploring the capability of synthesized PVP-oxime for corrosion inhibition of a mild steel surface in a 1 M H2SO4 solution. Portugaliae Electrochim Acta. 2020;38:43–58.
24. Kumar A. Comparative photocatalytic degradation of Rose Bengal dye under visible light by TiO2, TiO2/PAni and TiO2/PAni/GO nanocomposites. Int J Res Appl Sci Eng Technol. 2018;6:339–50.
25. Shimoga G, Palem RR, Choi DS, Shin EJ, Ganesh PS, Saratale GD, et al. Polypyrrole-based metal nanocomposite electrode materials for high-performance supercapacitors. Metals (Basel). 2021;11(6):905.
26. Yu H, He Y, Li H, Li Z, Ren B, Chen G et al. Core-shell PPy@TiO2 enable GO membranes with controllable and stable dye desalination properties. Desalination. 2022;526:115523.
27. Mubarak MF, Selim H, Elshypany R. Hybrid magnetic core–shell TiO_2@$CoFe_3O_4$ composite towards visible light-driven photodegradation of Methylene blue dye and the heavy metal adsorption: isotherm and kinetic study. J Environ Health Sci Eng. 2022;20:265–80.
28. Kim D, Kim KM, Han H, et al. Ti/TiO2/SiO2 multilayer thin films with enhanced spectral selectivity for optical narrow bandpass filters. Sci Rep. 2022;12. https://doi.org/10.1038/s41598-021-03935-z.
29. Abdi MM, Mohd Azli NFW, Lim HN, Tahir PM, Karimi G, Hoong YB et al. Polypyrrole/tannin biobased nanocomposite with enhanced electrochemical and physical properties. RSC Adv [Internet]. 2018;8:2978–85. Available from: https://doi.org/10.1039/C7RA13378B
30. Paul DR, Sharma R, Nehra SP, Sharma A. Effect of calcination temperature, pH and catalyst loading on photodegradation efficiency of urea derived graphitic carbon nitride towards methylene blue dye solution. RSC Adv R Soc Chem. 2019;9:15381–91.
31. Malik R, Lata S, Malik RS. Study of supercapacitive pursuance of polypyrrole/sulphonated poly (ether ether ketone) / multi walled carbon nanotubes composites for energy storage. J Energy Storage. 2020;27:101162.
32. Bengalli R, Ortelli S, Blosi M, Costa A, Mantecca P, Fiandra L. In vitro toxicity of TiO_2:SiO_2 nanocomposites with different photocatalytic properties. Nanomaterials. 2019;9(7):1041.
33. Balakrishnan M, John R. Impact of Ni metal ion concentration in TiO2 nanoparticles for enhanced photovoltaic performance of dye sensitized solar Cell. J Mater Sci Mater Electron. 2021;32:5295–308.
34. Wei Z, Zhou M, Qiao H, Zhu L, Yang H, Xia T. Particle size and pore structure characterization of silver nanoparticles prepared by confined arc plasma. J Nanomater. 2009;2009.
35. Kaur Sidhu G, Kumar R. Study the structural and optical behaviour of conducting polymer based nanocomposites: ZrO2-Polypyrrole nanocomposites. IOP Conf Ser Mater Sci Eng. Institute of Physics Publishing; 2018.
36. de Urquijo-Ventura MS, Rao MGS, Meraz-Davila S, Ochoa JAT, Quevedo-Lopez MA, Ramirez-Bon R. PVP-SiO2 and PVP-TiO2 hybrid films for dielectric gate applications in CdS-based thin film transistors. Polymer (Guildf). 2020;191:122261.
37. Uma K, Chen SW, KrishnaKumar B, Jeyaprabha C, Yang TCK, Lin JH. Enhanced photocatalytic activity of CdS nanostar decorated SiO2/TiO2 composite spheres and the simulation effect using FDTD model. Ionics (Kiel). 2021;27:397–406.
38. Kim D, Kim KM, Han H, Lee J, Ko D, Park KR et al. Ti/TiO2/SiO2 multilayer thin films with enhanced spectral selectivity for optical narrow bandpass filters. Sci Rep. 2022;12(1):32.
39. Hasanvandian F, Shokri A, Moradi M, Kakavandi B, Rahman Setayesh S. Encapsulation of spinel CuCo2O4 hollow sphere in V2O5-decorated graphitic carbon nitride as high-efficiency double Z-type nanocomposite for levofloxacin photodegradation. J Hazard Mater. 2022;423:127090.
40. Patidar D, Yadav A, Paul DR, Sharma A, Nehra SP. Nanohybrids cadmium selenide-reduced graphene oxide for improving photo-degradation of methylene blue. Physica E Low Dimens Syst Nanostruct. 2019;114:113560.
41. Paul DR, Sharma R, Panchal P, Nehra SP, Gupta AP, Sharma A. Synthesis, characterization and application of silver doped graphitic carbon nitride as photocatalyst towards visible light photocatalytic hydrogen evolution. Int J Hydrog Energy. 2020;45:23937–46.
42. Saravanan R, Shankar H, Prakash T, Narayanan V, Stephen A. ZnO/CdO composite nanorods for photocatalytic degradation of methylene blue under visible light. Mater Chem Phys. 2011;125:277–80.
43. Alkaim AF, Aljeboree AM, Alrazaq NA, Baqir SJ, Hussein FH, Lilo AJ. Effect of pH on adsorption and photocatalytic degradation efficiency of different catalysts on removal of methylene blue. Asian J Chem. 2014;26:8445–8.

44. Thiyagarajan S, Singh S, Bahadur D. Reusable sunlight activated photocatalyst Ag3PO4 and its significant antibacterial activity. Mater Chem Phys. 2016;173:385–94.
45. Rizzo L, Fiorentino A, Anselmo A. Effect of solar radiation on multidrug resistant E. coli strains and antibiotic mixture photodegradation in wastewater polluted stream. Sci Total Environ. 2012;427–428:263–8.
46. Yu S, Liu J, Zhu W, Hu ZT, Lim TT, Yan X. Facile room-temperature synthesis of carboxylated graphene oxide-copper sulfide nanocomposite with high photodegradation and disinfection activities under solar light irradiation. Sci Rep. 2015;5(1):16369.
47. Saini N, Pahuja P, Lgaz H, Chung IM, Selwal K, Singhal S et al. PVP oxime-TiO2 -adenine as a hybrid material: Decent synthesis and depiction with advanced theoretical measurements for anticorrosive behavior and antibacterial potentiality. J Mol Liq. 2019;278:438–51. Available from: https://doi.org/10.1016/j.molliq.2019.01.054
48. Maruthapandi M, Saravanan A, Luong JHT, Gedanken A. Antimicrobial properties of the polyaniline composites against pseudomonas aeruginosa and klebsiella pneumoniae. J Funct Biomater. 2020;11(3):59.
49. Khanmohammadi S, Karimian R, Mostafidi E, Tanomand A, Hajibonabi F, Edjlali L et al. Polythiophene/TiO2 and Polythiophene/ZrO2 Nanocomposites: Physical and Antimicrobial Properties against Common Infections drug delivery View project paclitaxel production using Taxus tissue culture View project Polythiophene/TiO 2 and polythiophene/ZrO 2 nanocomposites: physical and antimicrobial properties against common infections [Internet]. 2018. Available from: www.BiointerfaceResearch.com. Accessed 02 Aug 2018.
50. Mohsen RM, Morsi SMM, Selim MM, Ghoneim AM, El-Sherif HM. Electrical, thermal, morphological, and antibacterial studies of synthesized polyaniline/zinc oxide nanocomposites. Polym Bull [Internet]. 2019;76:1–21. Available from: https://doi.org/10.1007/s00289-018-2348-4
51. Sridhar BC, Gunvanthrao Yernale N, Prasad MVNA. Synthesis, spectral characterization, and antibacterial and antifungal studies of PANI/V2O5 nanocomposites. Int J Chem Eng. 2016; 2016:1–7.
52. Nisar P, Ali N, Rahman L, Ali M, Shinwari ZK. Antimicrobial activities of biologically synthesized metal nanoparticles: an insight into the mechanism of action. J Biol Inorg Chem. Springer Verlag; 2019;24:929–41.
53. Moradi M, Kakavandi B, Bahadoran A, Giannakis S, Dehghanifard E. Intensification of persulfate-mediated elimination of bisphenol A by a spinel cobalt ferrite-anchored g-C3N4 S-scheme photocatalyst: Catalytic synergies and mechanistic interpretation. Sep Purif Technol. 2022;285:120313.
54. Bharti B, Li H, Liu D, Kumar H, Manikandan V, Zha X et al. Efficient Zr-doped FS–TiO2/SiO2 photocatalyst and its performance in acrylonitrile removal under simulated sunlight. Appl Phys A. 2020;126:1–10.
55. Govindaraj R, Pandian SM, Ramasamy P, Mukhopadhyay S. Sol-gel synthesized mesoporous anatase titanium dioxide nanoparticles for dye sensitized solar cell (DSSC) applications. Bull Mater Sci. 2015;38:291–6.